THE JOURNAL OF PHYSICAL CHEMISTRY C

Article

pubs.acs.org/JPCC

Double Role of HMTA in ZnO Nanorods Grown by Chemical Bath Deposition

Vincenzina Strano,[†] Riccardo Giovanni Urso,[‡] Mario Scuderi,[§] Kingsley O. Iwu,[†] Francesca Simone,[†] Enrico Ciliberto,[‡] Corrado Spinella,[§] and Salvo Mirabella*[,†]

[†]MATIS IMM-CNR and Dipartimento di Fisica e Astronomia and [‡]Dipartimento di Scienze Chimiche, Università di Catania, via S. Sofia 64, 95123 Catania, Italy

[§]IMM-CNR, VIII strada 5, 95121 Catania, Italy

Supporting Information

ABSTRACT: ZnO nanorods (NRs) grown by chemical bath deposition (CBD) are among the most promising semiconducting nanostructures currently investigated for a variety of applications. Still, contrasting experimental results appear in the literature on the microscopic mechanisms leading to high aspect ratio and vertically aligned ZnO NRs. Here, we report on CBD of ZnO NRs using Zn nitrate salt and hexamethylenetetramine (HMTA), evidencing a double role of HMTA in the NRs growth mechanism. Beyond the well-established pH buffering activity, HMTA is shown to introduce a strong steric hindrance effect, biasing growth along the *c*-axis and ensuring the vertical arrangement. This twofold function of HMTA should be taken into account for avoiding detrimental phenomena such as merging or suppression of NRs, which occur at low HMTA concentration.

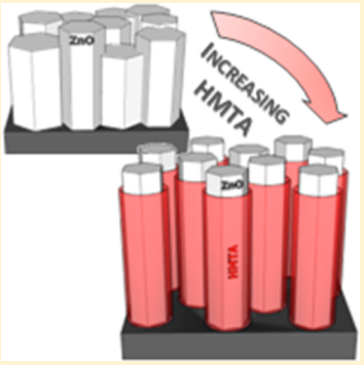

1. INTRODUCTION

Among semiconductor nanostructures, ZnO nanorods (NRs) recently emerged as promising building blocks in many applications such as piezoelectric transducers, photovoltaic devices, UV detectors, photocatalysis, gas and bio sensors, and light-emitting diodes.[1−12] This is due to both ZnO peculiar properties[13]—large and direct band gap energy of 3.3 eV, high exciton binding energy of 60 meV, high electron mobility, and large piezoelectric response—and the attractiveness of synthesizing ZnO NRs via low-cost methods based on solution phase growth. Among the bottom-up approaches, solution phase growth methods for nanostructures received much attention as they ensure high deposition rates on a large variety of substrate, without the need for high temperature or vacuum systems. In particular, chemical bath deposition (CBD) gained attention because of its simple experimental setup, cost effectiveness, and good potential for scaling up.

With respect to vacuum techniques, CBD, and solution phase synthesis methods in general, have the drawbacks of lack of good control over growth kinetics and unsatisfactory reproducibility from one laboratory to another, usually resulting in contrasting results reported in the literature. Such drawbacks can be even more severe when large scale production is attempted. Beyond the intrinsic limit of the solution phase techniques, there is also a partial understanding of the whole process underlying the growth of nanostructures. As far as the CBD growth of ZnO NRs is concerned, the role of the most used reducing agent, hexamethylenetetramine [HMTA $(CH_2)_6N_4$, a tertiary amine highly soluble in water], is currently under debate. This is despite the fact that a long series of papers has been published since its first utilization 30 years ago.[14−19] It is worth noting that the presence of HMTA is not essential for the ZnO nanorods growth,[19−21] but it ensures crystalline and morphological properties better than other reducing agents.

ZnO NRs growth by CBD occurs in an aqueous solution typically containing zinc nitrate and HMTA. After Zn nitrate dissociation, Zn^{2+} ion forms a complex with six water molecules $[Zn(H_2O)_6]^{2+}$, and essential equations for describing the ZnO NRs growth are the following:[16,19,22−24]

$$[Zn(H_2O)_6]^{2+} + H_2O \leftrightarrow [Zn(H_2O)_5OH]^{+} + H_3O^{+} \quad (1)$$

$$[Zn(H_2O)_5OH]^{+} + H_2O \leftrightarrow Zn(OH)_{2(s)} + H_3O^{+} + 4H_2O \quad (2)$$

$$Zn(OH)_{2(s)} \leftrightarrow ZnO_{(s)} + H_2O \quad (3)$$

while hydrolysis equilibria of $Zn^{2+}_{(aq)}$ move to the right for the simultaneous protonation of the HMTA itself or of the ammonia groups coming from HMTA decomposition:

$$(CH_2)_6N_4 + H_3O^{+} \leftrightarrow [(CH_2)_6N_4]H^{+} + H_2O \quad (4)$$

or

$$(CH_2)_6N_4 + 6H_2O \leftrightarrow 6HCHO + 4NH_3 \quad (5a)$$

Received: July 25, 2014
Revised: November 12, 2014
Published: November 12, 2014

 © 2014 American Chemical Society dx.doi.org/10.1021/jp507496a | J. Phys. Chem. C 2014, 118, 28189−28195

$$NH_3 + H_3O^+ \leftrightarrow NH_4^+ + H_2O \quad (5b)$$

If a rough or seeded substrate is immersed in that solution, well-ordered vertically oriented ZnO NRs can be grown on it.[22−24] The seed layer, which consists of zinc oxide crystallites preformed or spin-coated on the substrate,[25−27] promotes the heterogeneous nucleation on the substrate (while the homogeneous one typically occurs in the bulk solution). The fact that the anisotropic growth of these nanostructures is intrinsic to wet chemical methods and to wurtzite structure has found several experimental evidence.[28,29] However, on the precise role of HMTA there is not a general consensus. Govender et al.[30] first proposed that HMTA slowly releases the OH^- ions by its thermal decomposition to formaldehyde and ammonia. Ashfold et al.[31] reported that the rate of decomposition of HMTA at 90 °C calculated for a zinc-free solution is the same as that observed experimentally in a solution containing zinc nitrate and hexamethylenetetramine, implying that HMTA decomposition does not depend on the reactions taking place during ZnO deposition and that HMTA is an effective pH buffer. Although HMTA decomposition is assumed in most papers on CBD grown ZnO nanostructures,[32,33] Sugunan et al.[18] denied HMTA decomposition. By using attenuated total reflection Fourier transform infrared (ATR-FTIR) spectroscopy performed on a solution containing zinc nitrate and HMTA, Sugunan et al.[18] proposed that HMTA acts as a nonpolar chelating agent which preferentially attaches to the lateral (nonpolar) facets of ZnO NRs, inducing anisotropic growth along the *c*-axis. Such a shape-inducing effect of HMTA has been recently refuted by McPeak et al.,[19] who claim that ZnO nanorods growth by CBD does not involve the adsorption of HMTA on the ZnO lateral walls but that the role of HMTA is only to control the saturation index of ZnO through the slow release of OH^- ions. Thus, up to now it is not clear what the role of HMTA in ZnO NRs growth by CBD is.

In this work we present a systematic investigation of ZnO NRs grown by CBD involving Zn nitrate and HMTA. We report some empirical evidence to support the thesis that HMTA plays a dual role in the synthesis of ZnO nanorods on seeded substrate, participating both as supplier of OH^- and as capping agent promoting anisotropic growth. These two modes of action are not mutually exclusive, and the amount of HMTA in solution determines the key process variable.

2. EXPERIMENTAL SECTION

ZnO NRs were grown on c-Si substrate (2×2 cm^2 samples, cut from p-type, 4 in. Czochralski wafers) by CBD. After surface cleaning (isopropanol and acetone rinsing), a seed layer of ZnO crystallites was obtained by spin-coating (1000 rpm, 60 s) the surface with a solution of 5 mM zinc acetate dihydrate $(CH_3COO)_2Zn{\cdot}2H_2O$ (Sigma-Aldrich puriss. p.a., ACS reagent, ≥99.0%) in ethanol (Sigma-Aldrich puriss. p.a., ACS reagent, ≥99.8%), followed by 20 min annealing in air on a hot plate (at nominal 240 °C). This procedure gives about 2×10^{15} ZnO molecules/cm^2, clustered in small islands (average size of 23 nm, ∼60 nm away from each other), as detailed in the Supporting Information (Figure S1).

An open large beaker filled with a 100 mL solution (50 mM) of zinc nitrate hexahydrate ($Zn(NO_3)_2{\cdot}6H_2O$, Sigma-Aldrich purum p.a. crystallized, ≥99.0%) in deionized (DI) water (Milli-Q, 18 MΩ·cm) and a small beaker filled with 100 mL solution of varying HMTA concentration (Sigma-Aldrich puriss. p.a., Reag. Ph. Eur., ≥99.5%) in DI water were well stirred and preheated at 90 °C. The HMTA solution was poured into a large beaker, and the seeded substrates were vertically immersed in the large beaker. While zinc nitrate concentration in the CBD bath was set at 25 mM (after solution mixing), HMTA final concentration was varied in the 12.5−50 mM range. In some tests, HMTA was substituted or combined with propylamine (PA, $(CH_3)_3N$), a liquid primary amine.

As the concentrations of reactants vary with time (and at different specific rates), the solution aging effect can occur, decreasing the Zn^{2+}/OH^- ratio in a longer CBD process.[31,33] In addition, the temperature of the CBD solution heavily affects the growth kinetics.[30,34−36] These effects have to be considered when performing CBD experiments; thus, particular care was taken to immerse the substrates immediately after the solution mixing and to keep the solution temperature fixed at 90 °C through a boiling water bath (bain-marie configuration). Reaction time was varied in the range 0.5−3 h. pH and temperature were measured before, during (at 90 °C), and after the CDB with a pH-meter (EUTECH Instruments, pH2007) equipped with a temperature probe. Once the substrates were removed from the CBD beaker, they were rinsed with DI water and dried with N_2 gas.

The structural properties of ZnO nanostructures were studied by using a scanning electron microscope (Gemini field emission SEM Carl Zeiss SUPRA 25) and a transmission electron microscope (TEM, JEOL ARM200CF), operating in conventional TEM (CTEM) and diffraction mode.

3. RESULTS AND DISCUSSION

A. ZnO Nanorods Growth with HMTA. Figures 1a−c show the SEM analysis of ZnO NRs in plan (top panel) or cross view (bottom panel), evidencing that there is a strong dependence of the obtained morphology on the amount of HMTA used. All the samples were grown for 1 h at 90 °C, and the measured pH was 5.7. For 50 or 25 mM HMTA, a dense array of ZnO nanorods is obtained, with well-aligned and separated nanorods (40−50 nm wide, 600−700 nm high). The array is composed of ZnO nanorods with the well-known prism

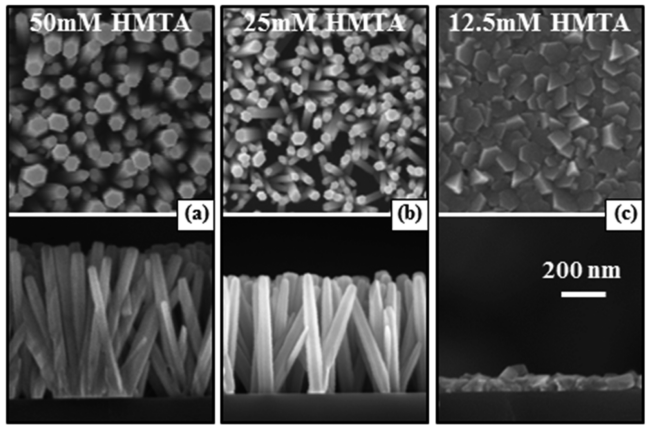

Figure 1. SEM images of the plane (top panel) and cross-sectional (bottom panel) views of the ZnO NRs grown with a zinc nitrate concentration of 25 mM and different molar concentrations of HMTA: 50 (a), 25 (b), and 12.5 mM (c). The growth temperature and time were 90 °C and 1 h, while the pH = 5.7. The scale bar is for all images.

dx.doi.org/10.1021/jp507496a | J. Phys. Chem. C 2014, 118, 28189−28195

shape and hexagonal section with a flat top. TEM analyses (discussed below) revealed that the growth direction is the *c*-axis, as expected. If 12.5 mM HMTA is used, a remarkably different structure is obtained, with ZnO platelets (100 nm wide and 80 nm high) merged with each other to form an almost continuous film. In this case, no anisotropic growth can be assumed as the height is even smaller than the lateral size, and moreover a large number of defects arose at the junction between these randomly oriented platelets. Thus, it is clear that there is a limit in the HMTA concentration over which the growth is biased toward the rodlike structure. Still, no difference in the pH of the solution is observed among the three cases; thus, the rodlike growth cannot be due to the OH^- release coming from the HTMA or ammonia protonation (eq 4 or 5). With 50 mM HMTA, ZnO NRs appear longer than in the case of 25 mM HMTA.

To compare the growth kinetics between 25 and 50 mM HMTA, we measured the height of NRs (by cross-view SEM) obtained from different durations of CBD. The results are reported in Figure 2 (error bars are of the same size as the

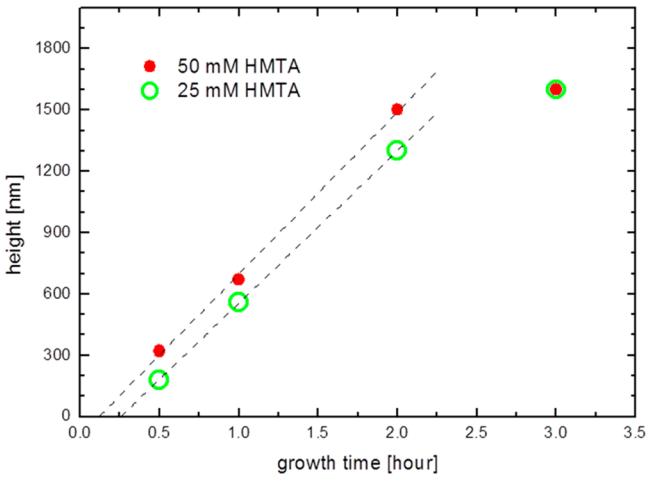

Figure 2. Time evolution of NRs height grown with 25 mM (open circles) or 50 mM (closed circles) HMTA concentration (Zn nitrate concentration of 25 mM, temperature of 90 °C, pH = 5.7). Lines are linear fit to extract growth rate and time offset, for data up to 2 h growth time.

symbols size). Several kinetics tests have been done, showing always the same results. For both HMTA concentrations, the NRs height scales linearly with growth time, up to a maximum time of 2 h. After this time the growth rate decreases, which can be related to the change in Zn^{2+} ions concentration in the solution after 2 h, as reported in ref 31. Thus, we preferred to focus our attention on the 0−2 h growth time interval. In this time range we observed no significant lateral growth, as the 25 mM HMTA samples show ZnO NRs as large as 40−50 nm from the beginning up to 2 h. The vertical growth rate can be determined with a simple linear fit for the 25 and 50 mM HMTA solutions, and it was found that the growth rate is fairly the same (12.5 nm/min for the 25 mM HMTA, 13.0 nm/min for the 50 mM HMTA). This means that by increasing the HMTA concentration, the hydrolysis equilibrium of $Zn^{2+}_{(aq)}$ is not significantly changed.

The difference in height of the ZnO NRs grown with different amount of HMTA is due essentially to a time offset before beginning of vertical growth (about 15.5 min for 25 mM and 7.2 min for 50 mM HMTA). The origin of this time offset is outside the scope of this work, even though we still observed the presence of ZnO NRs after 8 min growth with 25 mM HMTA, with a fairly low substrate coverage (Figure S2). Since the growth of ZnO NRs is shown to be transport limited, both height and lateral size of nanorods scale with the inverse of the nanorods density.[28] This implies that a linear trend in the vertical growth can be reached after an incubation time during which the NRs density becomes homogeneous on the whole surface. Given this picture, a large amount of HMTA in the growth solution ensures a shorter incubation time and, probably, a more homogeneous NRs array.

B. ZnO Nanorods Growth with PA. The role of the pH value in ZnO NR growth by CBD has been largely discussed,[11,14,15,19,22,30] concluding that by changing pH value different ZnO nanostructures can be formed. In this work, we always used pH value of 5.7, with HMTA as pH regulator. In order to clarify if HMTA has any other role beyond that of pH regulation, we replaced it with a simpler amine, propylamine (PA). pH regulation can also be achieved by using inorganic salt, but we decided not to use them as they are known to affect morphology of oxide nanostructures in low-temperature solution growth.

Figure 3a reports the pH values of a 25 mM solution of Zn nitrate kept at 90 °C with different concentration of HMTA or

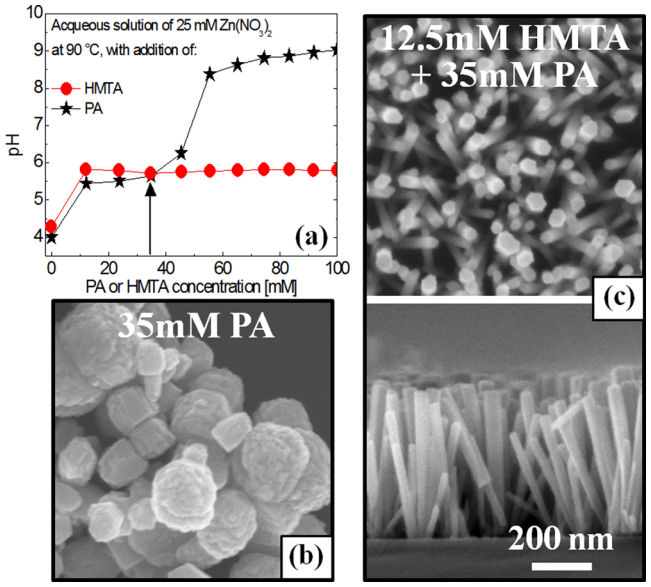

Figure 3. (a) pH measured in an aqueous solution of Zn nitrate (25 mM) kept at 90 °C with different concentration of HMTA (close circles) or PA (stars). (b) SEM plan view ZnO nanostructures grown with 35 mM PA (Zn nitrate concentration of 25 mM, temperature of 90 °C, growth time of 1 h, pH = 5.7). (c) SEM images of the plane (top panel) and cross-sectional (bottom panel) views of the ZnO NRs grown with 12.5 mM HMTA and 35 mM PA (Zn nitrate concentration of 25 mM, temperature of 90 °C, growth time of 1 h, pH = 5.7). The scale bar is for all images.

PA. Without any amine, the Zn nitrate solution is acidic (pH = 4.2) due to the hydrolysis of $Zn^{2+}_{(aq)}$ complex. HMTA shows a strong pH regulation activity, quickly stabilizing the pH at 5.7 in the 12.5−125 mM HMTA concentration range. The behavior of PA at low concentration is similar, while for PA concentration larger than 50 mM pH increases up to 9. In particular, a 35 mM PA solution has a pH = 5.7 (vertical arrow

dx.doi.org/10.1021/jp507496a | J. Phys. Chem. C 2014, 118, 28189−28195

in Figure 3a). In principle, if the role of HMTA is only to keep the pH = 5.7, using another reagent capable of ensuring the same pH condition should permit the synthesis of zinc oxide nanostructures with morphological features similar to those obtained by employing HMTA. Figure 3b shows the plan view of the CBD with 25 mM zinc nitrate and 35 mM PA solution. No nanorods or platelet structures were found. Given this results, we tried to repeat the growth by adding a small amount of HMTA. Figure 3c reports the SEM images in plan (top panel) and cross (bottom panel) of the ZnO nanorods obtained combining 35 mM PA and 12.5 mM HMTA (with a fixed 25 mM Zn nitrate). Under such conditions, very high and thin ZnO nanorods were obtained. It is worth noting that the same amount of HMTA (without PA) gave the merged ZnO platelets (Figure 1c). This indicates that ZnO NRs can be obtained even if a low amount of HMTA is used, as long as another pH regulator is present.

Figure 4 provides a synoptic view of the morphological features of ZnO NRs grown with different concentration of

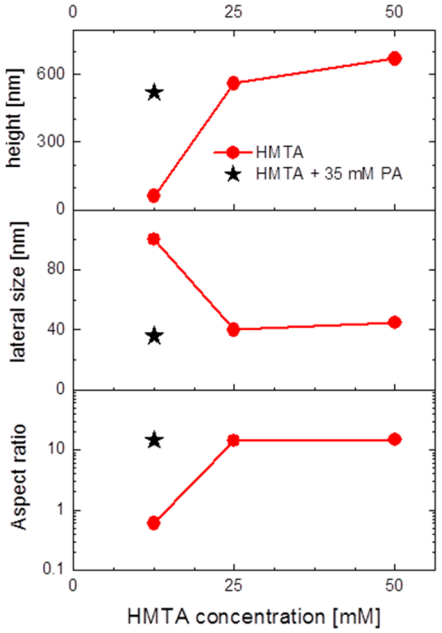

Figure 4. Circles refer to height (top), lateral sizes (medium), and aspect ratio (bottom) of ZnO NRs grown with different HMTA concentrations. Stars refer to ZnO NRs grown with HMTA (12.5 mM) and PA (35 mM). In all cases, Zn nitrate concentration was 25 mM, temperature was 90 °C, growth time 1 h, and pH = 5.7.

HMTA, with and without PA. The height and the lateral size were extracted from SEM images (error bars are of the same size as the symbols size). When only HMTA is used, higher HMTA concentration leads to significant increase in aspect ratio (AR), ranging from about 0.7 (12.5 mM HMTA) to about 15 (50 mM HMTA). The combination of PA and 12.5 mM HMTA (stars) leads to height, lateral size, and AR comparable to those obtained with higher amount of HMTA.

This effect of PA can be explained if a double role of HMTA is assumed—primarily it is a pH regulator, while its secondary role is to induce the rodlike growth of ZnO. In fact, looking at Figure 3a, 12.5 mM HMTA turns out to be high enough to maintain pH at 5.7, but in this case no ZnO nanorods are obtained, implying that most or all of the HMTA is used up in pH regulation. When more HMTA or PA is added, ZnO nanorods appear.

HMTA secondary function of biasing anisotropic growth of ZnO along the *c*-axis can be related to the preferential attachment of chelating HMTA molecules to the lateral faces of ZnO NRs.[18] HMTA can bind to nonpolar ZnO crystal surfaces by means of at least two mechanisms: a dative covalent bond between the basic N donor atoms and the acidic Zn^{2+} site or a hydrogen bonding between the tertiary ammonium cations and the O^{2-} crystal ions.[37] Any of them can lead to a steric hindrance effect, according to which NRs close enough to each other tend to inhibit lateral growth.[36,38,39] This explanation is in apparent contrast with the conclusion of ref 19 where it is stated that HMTA does not adsorb on ZnO nanoparticles film. However, they used very low HMTA concentration (1 mM), and the HMTA absorption test was carried out at temperature well below 90 °C. At these conditions, HMTA adsorption and bonding to ZnO may not be favorable. Our results indicate that for typical ZnO NR growth condition (90 °C, pH = 5.7, HMTA = 25 mM) a clear steric hindrance effect induced by HMTA cannot be ruled out.

C. Steric Hindrance Effect during ZnO NRs Growth. TEM analysis were performed on ZnO NRs grown with 25 or 50 mM HMTA or with the combination of 12.5 mM HMTA and 35 mM PA. In order to study the morphology of the NRs below the surface of the film, the NRs array was embedded by using an epoxy resin and then sliced up, extracting a plane of observation about 100 nm above the substrate. All TEM images refer to this kind of slice. Figure 5 shows the bright field

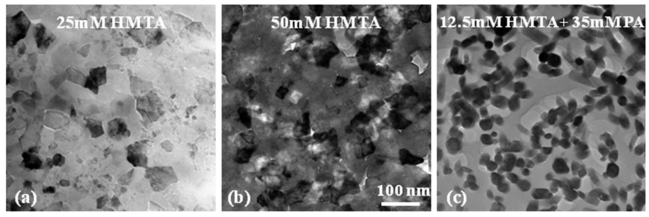

Figure 5. TEM images of a slice extracted 100 nm above the substrate of ZnO NRs samples grown with 25 mM HMTA (a), 50 mM HMTA (b), or 12.5 mM HMTA+35 mM PA (c) (Zn nitrate concentration of 25 mM, temperature of 90 °C, growth time of 1 h, pH = 5.7). The scale bar is for all images.

transmission electron microscopy (BF-TEM) images of ZnO NRs grown with 25 mM (Figure 5a), 50 mM (Figure 5b) of HMTA, or with the combination of 12.5 mM HMTA and 35 mM PA (Figure 5c). NRs with [0001] zone axis aligned with the line of sight appear with darker contrast and sharper edges. As shown by SEM images in Figure 1, not all NRs are properly perpendicular to the substrate, so some misalignment occurs. Selected area diffraction (SAD) patterns of TEM (presented in Figure S3) show that NRs are wurtzite ZnO crystals with a predominant [0001] growth direction.

It is clear that large differences arose among the three samples. All of them shows quite large NR density, though the HMTA + PA sample has by far the less dense arrangement of NRs. Furthermore, the 25 mM HMTA sample presents both smaller and larger NRs while the 50 mM HMTA and the HMTA + PA samples have more uniformly sized NRs.

In order to investigate this point, we calculated the size distribution (Figure 6) of ZnO NRs both on the top plane and at 100 nm (bottom plane, hereafter) above the substrate, using

dx.doi.org/10.1021/jp507496a | J. Phys. Chem. C 2014, 118, 28189−28195

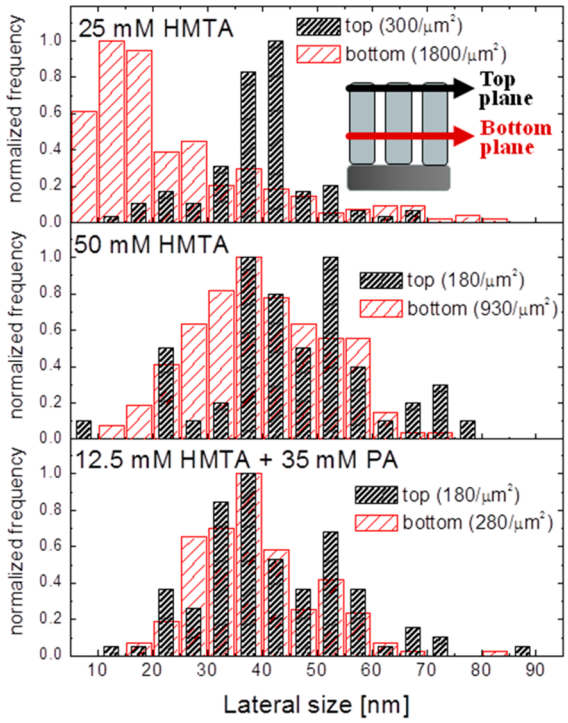

Figure 6. Size distribution of ZnO NRs in samples grown with 25 mM HMTA (a), 50 mM HMTA (b), or 12.5 mM HMTA+35 mM PA (c) (Zn nitrate concentration of 25 mM, temperature of 90 °C, growth time of 1 h, pH = 5.7). Black and red histograms refer to the top or bottom (100 nm above the substrate) planes, as depicted in the drawing. NRs density per μm^2 are also reported in the legend for each sample, at the bottom and top planes.

SEM images in Figures 1 and 3 and TEM images in Figure 5, respectively. Although two different techniques have been used on top and bottom of NRs, a fair comparison can be done and many reliable information can be drawn. For each sample, the areal density of NRs is reported, for both planes. In the case of only HMTA, the NR density clearly decreases from the bottom plane to the top one, in particular for the 25 mM HMTA sample. The same sample, moreover, shows a markedly larger size distribution at the bottom plane in comparison to all the other samples. Such a situation can also be related to the larger incubation time extracted for this same sample (Figure 2), as a longer nucleation time typically gives a larger size distribution. In addition, with 25 mM HMTA, the most representative size (35−40 nm) at the top plane is larger than the most representative size (10−20 nm) at the bottom plane. This may indicate that most of the ZnO NRs present at the bottom do not reach the top plane, perhaps suppressed during the growth. Another explanation is that merging of small NRs probably occurred (Figure S4) by means of crystal coarsening or oriented attachment.[40] The 50 mM HMTA NRs behaves slightly different, as the average size slightly increases from the bottom to the top plane, with a decrease of the NR density. The HMTA + PA sample shows fairly the same average size among the two planes, with only a moderate reduction in the NR density. It should be noted that this sample shows the lowest reduction in NRs density going from the bottom to the top plane and that also at the bottom plane the NRs density is quite low (see Figure 5c). In general, ZnO NRs growth in this case seemed to occur without any merging or NR suppression.

These results can be interpreted with the steric hindrance effect. Basically, there is a sort of dynamic equilibrium among attached molecules (HMTA*) and molecules dispersed in solution. When only 25 mM HMTA is used, the HMTA concentration in the residual solution at the bottom part of NRs during the growth becomes less and less, shifting the equilibrium toward molecules dispersed in solution. This reduces the HMTA* amount and consequently the steric hindrance effect. Merging phenomena can then occur. As the HMTA is increased, a more controlled growth occurs with 50 mM HMTA or even better with the HMTA + PA combination.

To counterprove the HMTA-induced steric hindrance action, a double-step synthesis test was carried out with HMTA concentration varied during the growth. Two seeded substrates were immersed in an equimolar solution (25 mM) of zinc nitrate and HMTA at 90 °C (pH = 5.7). After 1 h, one sample was extracted, rinsed, and dried, and a solution of 25 mM zinc nitrate (preheated heated at 90 °C) was added to double the original volume. The nominal HMTA concentration was then halved (12.5 mM) while maintaining that of zinc nitrate at 25 mM. The diluted solution had pH = 5.7, as expected. The second substrate was kept in the diluted solution for a further 30 min, then removed, rinsed, and dried. Figure 7 reports the

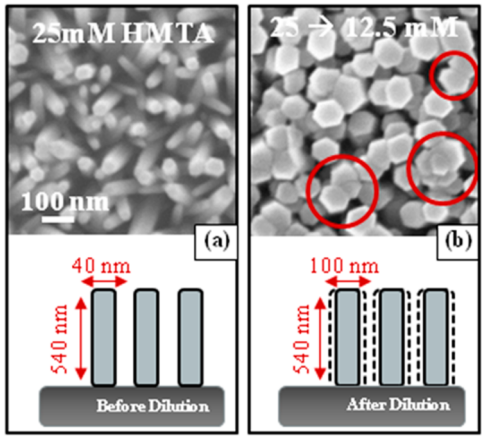

Figure 7. SEM plan views of ZnO NRs grown with 25 mM HMTA for 1 h (a) or with 25 mM HMTA for 1 h plus 12.5 mM HMTA for further 30 min (b) (Zn nitrate concentration of 25 mM, temperature of 90 °C, pH = 5.7). Red circles indicate merging ZnO NRs, while drawings below represent height and lateral size of NRs before and after HMTA dilution. The scale bar is for all images.

results of this double-step synthesis test. After the first growth, ZnO NRs (Figure 7a) exhibit an average lateral size of 40 nm and a height of 540 nm. The second step (Figure 7b) surprisingly did not give any extra height (as observed by cross SEM images, not reported) but only a significant lateral size growth (from 40 to 100 nm), with several evidence of NR merging (red circles in Figure 7b). This scenario further confirms the steric hindrance action of HMTA, giving an explicit evidence that the NRs anisotropic growth strongly depends on the HMTA concentration. After the dilution, the amount of HMTA becomes so low that growth along the *c*-axis is essentially suppressed while only lateral growth occurs on the side walls of NRs.

dx.doi.org/10.1021/jp507496a | J. Phys. Chem. C 2014, 118, 28189−28195

4. CONCLUSIONS

In conclusion, we experimentally studied the role of HMTA in the chemical bath deposition of ZnO nanorods using a 25 mM zinc nitrate aqueous solution. It is clearly shown that a lower threshold in the HMTA concentration exists in order to induce the anisotropic growth of ZnO NRs along the *c*-axis. Increasing the HMTA concentration does not increase the growth rate of NRs. ZnO NRs can be obtained with a lower HMTA concentration only if another pH regulator is involved. These data point out that HMTA plays a double role, acting as pH regulator, and forming a shell around ZnO NR. The last effect induces the vertical growth of ZnO NR along the *c*-axis through a steric hindrance effect, inhibiting lateral growth. When low HMTA concentration are used, detrimental effects such as NRs merging or enhanced lateral growth occur.

■ ASSOCIATED CONTENT

Supporting Information

SEM, TEM, and RBS of seeded substrate; early stage of NR growth and of merged NRs occurrence. This material is available free of charge via the Internet at http://pubs.acs.org.

■ AUTHOR INFORMATION

Corresponding Author

*Tel +39-095-3785438; Fax +39-095-3785243; e-mail mirabella@ct.infn.it (S.M.).

Author Contributions

V.S. conceived the study and contributed to sample synthesis, SEM analyses, data interpretation, and manuscript drafting. R.G.U. conceived the study and contributed to sample synthesis and data interpretation. M.S. and C.S. provided TEM analyses. K.O.I., F.S., and E.C. contributed to data interpretation and manuscript revision. S.M. conceived the study and contributed to analyses, data interpretation, and manuscript revision. All authors have given approval to the final version of the manuscript.

Notes

The authors declare no competing financial interest.

■ ACKNOWLEDGMENTS

This work has been partially sponsored by the project PLAST_ICs (PON02_00355_3416798 PON 2007−2013). The authors thank E. G. Barbagiovanni and I. Crupi (MATIS CNR-IMM) for scientific discussions and G. Panté, S. Tatì (MATIS CNR-IMM), and A. Rapicavoli (Univ. of Catania) for expert technical assistance.

■ REFERENCES

(1) Wang, Z. L.; Song, J. Piezoelectric Nanogenerators Based on Zinc Oxide Nanowire Arrays. *Science* **2006**, *312*, 242−246.

(2) Zhou, J.; Gu, Y.; Fei, P.; Mai, W.; Gao, Y.; Yang, R.; Bao, G.; Wang, Z. L. Flexible Piezotronic Strain Sensor. *Nano Lett.* **2008**, *8*, 3035−3040.

(3) Law, M.; Greene, L. E.; Johnson, J. C.; Saykally, R.; Yang, P. Nanowire Dye-Sensitized Solar Cells. *Nat. Mater.* **2005**, *4*, 455−459.

(4) Shinagawa, T.; Shibata, K.; Shimomura, O.; Chigane, M.; Nomura, R.; Izaki, M. Solution-Processed High-Haze ZnO Pyramidal Textures Directly Grown on a TCO Substrate and the Light-Trapping Effect in Cu_2O Solar Cells. *J. Mater. Chem. C* **2014**, *2*, 2908−2917.

(5) Pradhan, B.; Batabyal, S. K.; Pal, A. J. Vertically Aligned ZnO Nanowire Arrays in Rose Bengal-Based Dye-Sensitized Solar Cells. *Sol. Energy Mater. Sol. Cells* **2007**, *91*, 769−773.

(6) Sang, L.; Liao, M.; Sumiya, M. A Comprehensive Review of Semiconductor Ultraviolet Photodetectors: From Thin Film to One-Dimensional Nanostructures. *Sensors* **2013**, *13*, 10482−10518.

(7) Hassan, J. J.; Mahdi, M. A.; Kasim, S. J.; Ahmed, N. M.; Hassan, H. A.; Hassan, Z. High Sensitivity and Fast Response and Recovery Times in a ZnO Nanorod Array/p-Si Self-Powered Ultraviolet Detector. *Appl. Phys. Lett.* **2012**, *101*, 261108.

(8) Tian, T.; Zhang, Q.; Wu, A.; Jiang, M.; Liang, Z.; Jiang, B.; Fu, H. Cost-Effective Large-Scale Synthesis of ZnO Photocatalyst with Excellent Performance for Dye Photodegradation. *Chem. Commun.* **2012**, *48*, 2858−2860.

(9) Alenezi, R. M.; Alshammari, A. S.; Jayawardena, K. D. G. I.; Beliatis, M. J.; Henely, S. J.; Silva, S. R. P. Role of the Exposed Polar Facets in the Performance of Thermally and UV Activated ZnO Nanostructured Gas Sensors. *J. Phys. Chem. C* **2013**, *117*, 17850−17858.

(10) Al-Hilli, S.; Willander, M. The pH Response and Sensing Mechanism of n-Type ZnO/Electrolyte Interfaces. *Sensors* **2009**, *9*, 7445−7480.

(11) Joo, J.; Chow, B. Y.; Prakash, M.; Boyden, E. S.; Jacobson, J. M. Face-Selective Electrostatic Control of Hydrothermal Zinc Oxide Nanowire Synthesis. *Nat. Mater.* **2011**, *10*, 596−601.

(12) Shoaee, S.; Briscoe, J.; Durrant, J.; Dunn, S. Acoustic Enhancement of Polymer/ZnO Nanorod Photovoltaic Device Performance. *Adv. Mater.* **2014**, *26*, 263−268.

(13) Janotti, A.; Vand de Walle, C. G. Fundamentals of Zinc Oxide as a Semiconductor. *Rep. Prog. Phys.* **2009**, *72*, 12650.

(14) Fujita, K.; Murata, K.; Nakazawa, T.; Kayama, I. Crystal Shape of Zinc Oxide Prepared by the Homogeneous Precipitation Method. *Yogyo Kyokaishi* **1984**, *92*, 227−230.

(15) Andres Verges, M.; Mifsud, A.; Serna, C. J. Formation of Rod-like Zinc Oxide Microcrystals in Homogeneous Solution. *J. Chem. Soc., Faraday Trans.* **1990**, *86*, 959−963.

(16) Vayssieres, L.; Keis, K.; Lindquist, S. E.; Hagfeldt, A. Purpose-Built Anisotropic Metal Oxide Material: 3D Highly Oriented Microrod Array of ZnO. *J. Phys. Chem. B* **2001**, *105*, 3350−3352.

(17) Greene, L. E.; Law, M.; Goldberger, J.; Kim, F.; Johnson, J. C.; Zhang, Y.; Sayakally, R. J.; Yang, P. Low-Temperature Wafer-Scale Production of ZnO Nanowire Arrays. *Angew. Chem., Int. Ed.* **2003**, *42*, 3031−3034.

(18) Sugunan, A.; Warad, H. C.; Boman, M.; Dutta, J. Zinc Oxide Nanowires in Chemical Bath on Seeded Substrate: Role of Hexamine. *J. Sol-Gel Sci. Technol.* **2006**, *39*, 49−56.

(19) McPeak, K. M.; Le, T. P.; Britton, N. G.; Nickolov, Z. S.; Elabd, Y. A.; Baxter, J. B. Chemical Bath Deposition of ZnO Nanowires at Near-Neutral pH Conditions without Hexamethylenetetramine (HMTA) in ZnO Nanowire Growth. *Langmuir* **2011**, *27*, 3672−3677.

(20) Khusaimi, Z.; Mamat, M. H.; Sahdan, M. Z.; Abdullah, N.; Rusop, M. *Defect Diffus. Forum* **2011**, *312−315*, 99−103.

(21) Li, W. J.; Shi, E. W.; Zhong, W. Z.; Yin, Z. W. Growth Mechanism and Growth Habit of Oxide Crystals. *J. Cryst. Growth* **1999**, *203*, 186−196.

(22) Baruah, S.; Dutta, J. Effect of Seeded Substrate on Hydrothemally Grown ZnO Nanorods. *J. Sol-Gel Sci. Technol.* **2009**, *50*, 456−464.

(23) Guillemin, S.; Consonni, V.; Appert, E.; Puyoo, E.; Rapenne, L.; Roussel, H. Critical Nucleation Effects on the Structural Relationship Between ZnO Seed Layer and Nanowires. *J. Phys. Chem. C* **2012**, *116*, 25106−25111.

(24) Guillemin, S.; Rapenne, L.; Roussel, H.; Sarigiannidou, E.; Bremond, G.; Consonni, V. Formation Mechanismo of ZnO Nanowires: The Crucial Role of Crystal Orientatio and Polarity. *J. Phys. Chem. C* **2013**, *117*, 20738−20745.

(25) Greene, L. E.; Law, M.; Tan, D. H.; Montano, M.; Goldberger, J.; Somorjai, G.; Yang, P. General Route to Vertical ZnO Nanowire Arrays Using Textured ZnO Seeds. *Nano Lett.* **2005**, *5*, 1231−1236.

(26) Hu, X.; Masuda, Y.; Ohji, T.; Kato, K. In situ Forced Hydorlysis-Assisted Fabrication and Photo-induced Electrical Property in Sensor of ZnO Nanoarrays. *J. Colloid Interface Sci.* **2008**, *325*, 459−463.

(27) Ghayour, H.; Rezaie, H. R.; Mirdamadi, Sh.; Nourbakhsh, A. A. The Effect of Seed Layer Thickness on Alignment and Morphology of ZnO Nanorods. *Vaccum* **2011**, *86*, 101−105.
(28) Boercker, J. E.; Schmidt, J. B.; Aydil, E. Transport Limited Growth of Zinc Oxide Nanowires. *Cryst. Growth Des.* **2009**, *9*, 2783−2789.
(29) Xu, S.; Shen, Y.; Ding, Y.; Wang, Z. L. Growth and Transfer of Monolithic Horizontal ZnO Nanowire Superstructures onto Flexible Substrates. *Adv. Funct. Mater.* **2010**, *20*, 14793−1497.
(30) Govender, K.; Boyle, D. S.; Kenway, P. B.; O'Brien, P. Understanding the Factors that Govern the Deposition and Morphology of Thin Films of ZnO from Aqueous Solution. *J. Mater. Chem.* **2004**, *14*, 2575−2591.
(31) Ashfold, M. N. R.; Doherty, R. P.; Ndifor-Angwafor, N. G.; Riley, D. J.; Sun, Y. The Kinetics of Hydrothermal Growth of ZnO Nanostructures. *Thin Solid Fims* **2007**, *515*, 8679−8683.
(32) Qiu, J.; Li, X.; He, W.; Park, S. J.; Kim, H. K.; Hwang, Y. H.; Lee, J. H.; Kim, Y. D. The Growth Mechanism and Optical Properties of Ultralong ZnO Nanorod Arrays with a High Aspect Ratio by a Preheating Hydrothermal Method. *Nanotechnology* **2009**, *20*, 155603.
(33) Sun, Y.; Riley, J.; Ashfold, M. N. R. Mechanism of ZnO Nanotube Growth by Hydrothemal Methods on ZNO Film- Coated Si Substrates. *J. Phys. Chem. B* **2006**, *110*, 15186−15192.
(34) Guo, M.; Diao, P.; Cai, S. Hydrothermal Growth of Well-Aligned ZnO Nanorod Arrays: Dependendence of Morphology and Alignment Ordering upon Preparing Conditions. *J. Solid State Chem.* **2005**, *178*, 1864−1873.
(35) Wang, S. F.; Tseng, T. Y.; Wang, Y. R.; Wang, C. Y.; Lu, H. C.; Shih, W. L. Effect of Preparation Conditions in the Growth of ZnO Nanorod Arrays Using Aqueous Solution Method. *Int. J. Appl. Cer. Technol.* **2008**, *5*, 419−429.
(36) Singh, D.; Narasimulu, A. A.; Garcia-Gancedo, L.; Fu, Y. Q.; Soin, N.; Shao, G.; Luo, J. K. Novel ZnO Nanorod Films by Chemical Solution Deposition for Planar Device Applications. *Nanotechnology* **2013**, *24*, 275601.
(37) Schomaker, V.; Shaffer, P. A., Jr. A Reinvestigation of Hexamethylenetetramine by Electron Diffraction. *J. Am. Chem. Soc.* **1947**, *69*, 1555−1557.
(38) Ren, Z. F.; Huang, Z. P.; Xu, J. W.; Wang, J. H.; Bush, P.; Siegal, M. P.; Provencio, P. N. Synthesis of Large Arrays of Well-Aligned Carbon Nanotubes on Glass. *Science* **1998**, *282*, 1105−1107.
(39) Lee, C. J.; Kim, D. W.; Lee, T. J.; Choi, Y. C.; Park, Y. S.; Lee, Y. H.; Choi, W. B.; Lee, N. S.; Park, G. S.; Kim, J. M. Synthesis of Aligned Carbon Nanotubes Using Thermal Chemical Vapor Deposition. *Chem. Phys. Lett.* **1999**, *312*, 461−468.
(40) Zhang, Q.; Liu, S. J.; You, S. H. Recent Advances in Oriented Attachment Growth and Synthesis of Functional Materials: Concept, Evidence, Mechanism and Future. *J. Mater. Chem.* **2009**, *19*, 191−207.